Journal of Visualized Experiments

3D Particle Tracking for Noninvasive In Vivo Analysis of Synaptic Microtubule Dynamics in Dendrites and Neuromuscular Junctions of Drosophila

--Manuscript Draft--

Article Type:	Methods Article - JoVE Produced Video
Manuscript Number:	JoVE61159R1
Full Title:	3D Particle Tracking for Noninvasive In Vivo Analysis of Synaptic Microtubule Dynamics in Dendrites and Neuromuscular Junctions of Drosophila
Section/Category:	JoVE Neuroscience
Keywords:	Drosophila melanogaster; neuron; microtubule; Synapse; dendrite; neuromuscular junction; time-lapse imaging; Live imaging; particle tracking; quantitative analysis; transforming acidic coiled coil protein.
Corresponding Author:	Vivian Tsai-Wei Chou Harvard Medical School Boston, MA UNITED STATES
Corresponding Author's Institution:	Harvard Medical School
Corresponding Author E-Mail:	vtchou@gmail.com
Order of Authors:	Vivian Tsai-Wei Chou
	Hunkar Gizem Yesilyurt
	Hoyin Lai
	Jennifer B. Long
	Mercedes Arnes
	Kamal Obbad
	Michael Jones
	Hideki Sasaki
	Luciano A.G. Lucas
	Sam Alworth
	James Shih-Jong Lee
	David Van Vactor
Additional Information:	
Question	**Response**
Please indicate whether this article will be Standard Access or Open Access.	Standard Access (US$2,400)
Please indicate the **city, state/province, and country** where this article will be **filmed**. Please do not use abbreviations.	Boston, Massachusetts, United States

TITLE:

3D Particle Tracking for Noninvasive In Vivo Analysis of Synaptic Microtubule Dynamics in Dendrites and Neuromuscular Junctions of Drosophila

AUTHORS AND AFFILIATIONS:

Vivian T. Chou[1,*], Hunkar Gizem Yesilyurt[1,*], Hoyin Lai[2,*], Jennifer Long[1], Mercedes Arnes[1], Kamal Obbad[1], Michael Jones[2], Hideki Sasaki[2], Luciano A.G. Lucas[2], Sam Alworth[2], James Shih-Jong Lee[2], David Van Vactor[1]

[1]Blavatnik Institute of Cell Biology and Program in Neuroscience, Harvard Medical School, Boston, MA

[2]DRVision Technologies LLC, Bellevue, WA

*These authors contributed equally

Corresponding Author:

David Van Vactor (davie_vanvactor@hms.harvard.edu)

Author Email Addresses:

Vivian T. Chou (vtchou@gmail.com)
Hunkar Gizem Yesilyurt (HunkarGizem_Yesilyurt@hms.harvard.edu)
Hoyin Lai (hoyinl@drvtechnologies.com)
Jennifer Long (jgatti@bbns.org)
Mercedes Arnes (ma3661@cumc.columbia.edu)
Kamal Obbad (kobbad@college.harvard.edu)
Michael Jones (michaelj@drvisiontechnologies.com)
Hideki Sasaki (hidekis@drvisiontechnologies.com)
Luciano A.G. Lucas (lucianol@drvisiontechnologies.com)
Sam Alworth (salworth@acurastem.com)
James Shih-Jong Lee (jamesl@drvisiontechnologies.com)

KEYWORDS:

Drosophila melanogaster, neuron, microtubule, synapse, dendrite, neuromuscular junction, time-lapse imaging, live imaging, particle tracking, quantitative analysis, transforming acidic coiled coil protein

SUMMARY:

This study presents a noninvasive intravital neuronal imaging strategy combined with a new software strategy to achieve automated, unbiased tracking and analysis of in vivo microtubule (MT) plus-end dynamics in the sensory dendrites and the neuromuscular junctions of Drosophila.

ABSTRACT:

Microtubules (MTs) play critical roles in neuronal development, but many questions remain

about the molecular mechanisms of their regulation and function. Furthermore, despite progress in understanding postsynaptic MTs, much less is known about the contributions of presynaptic MTs to neuronal morphogenesis. In particular, studies of in vivo MT dynamics in Drosophila sensory dendrites yielded significant insights into polymer-level behavior. However, the technical and analytical challenges associated with live imaging of the fly neuromuscular junction (NMJ) have limited comparable studies of presynaptic MT dynamics. Moreover, while there are many highly effective software strategies for automated analysis of MT dynamics in vitro and ex vivo, in vivo data often necessitate significant operator input or entirely manual analysis due to inherently inferior signal-to-noise ratio in images and complex cellular morphology. To address this, this study optimized a new software platform for automated and unbiased in vivo particle detection. Multiparametric analysis of live time-lapse confocal images of EB1-GFP labeled MTs was performed in both dendrites and the NMJ of Drosophila larvae and found striking differences in MT behaviors. MT dynamics were furthermore analyzed following knockdown of the MT-associated protein (MAP) dTACC, a key regulator of Drosophila synapse development, and identified statistically significant changes in MT dynamics compared to wild type. These results demonstrate that this novel strategy for the automated multiparametric analysis of both pre- and postsynaptic MT dynamics at the polymer-level significantly reduces human-in-the-loop criteria. The study furthermore shows the utility of this method in detecting distinct MT behaviors upon dTACC-knockdown, indicating a possible future application for functional screens of factors that regulate MT dynamics in vivo. Future applications of this method may also focus on elucidating cell type and/or compartment-specific MT behaviors, and multicolor correlative imaging of EB1-GFP with other cellular and subcellular markers of interest.

INTRODUCTION:

Cells organize to form functional structures through the coordination of intra- and intercellular changes via morphogenesis. A remarkable example of morphogenesis is the development of the highly specialized neuronal structure. Neurons display remarkable polarization, in which they extend two structurally and functionally distinct types of processes, dendrites and axons[1], which can achieve immense lengths. The complexity of neuronal development arises not only from the sheer size of dendrites and axons but also from the difficulty in forming their intricately branched geometries[2,3]. Neuronal morphogenesis and its consequences in learning and memory[4] motivate the ongoing investigation of both its genetic control and the underlying cell biological mechanisms. Such mechanisms include, but are not limited to, intracellular membrane transport and the many cytoskeletal rearrangements needed for changes in neuronal morphology[1–3].

Studies of neuronal morphogenesis have produced a variety of advanced visualization techniques. Static methods, such as electron microscopy or fluorescence microscopy of fixed probes, are widely used to perform high-resolution morphological and structural analysis. However, besides the artifacts that are inevitable to any preservation method, static visualization cannot capture the dynamic changes that underpin morphogenesis. Thus, many pivotal insights originated from time-lapse fluorescence microscopy of living tissues. Early work by Lichtman and colleagues[5–7] utilized in vivo imaging of the mammalian nervous system to investigate axon regeneration/degeneration, organization of synaptic components, and long-range axonal transport. Furthermore, seminal studies in primary neuronal explants were critical to establishing

the importance of microtubule (MT) dynamics to axonal elongation and motility[8,9]. Crucially, early neuronal explant studies established the use of fluorescently-tagged end-binding family proteins (EBs) to gain invaluable insights into MT plus-end dynamics in developing neurons at the level of individual MT polymers[10]. These studies arose from observations that the EB family member EB1 preferentially localizes to MT plus ends[11] in S. cerevisiae[12] and in cultured cells[13]. Since then, EB1 and other plus tip tracking proteins (+TIPs)[14,15] have been widely used in in vivo studies of MT dynamic instability[16], including in the context of neuronal development[17].

Drosophila is a powerful model for in vivo imaging studies of MT dynamics during neuronal development due to the vast genetic and imaging tools available for fly studies[18,19] as well as the similarities in structure and function between Drosophila and vertebrate neurons[1]. A key early study of the neuromuscular junction (NMJ) of Drosophila larvae performed repeated noninvasive imaging of a fluorescent membrane marker through the translucent cuticle of intact animals to document presynaptic terminal morphogenesis[20]. Using a similar method to image whole, live Drosophila larvae, an initial demonstration of subcellular, particle-level analysis of processive movement of motor cargos in the axons was provided[21]. More recently, meticulous studies by Rolls and colleagues in the sensory dendrites of intact Drosophila larvae[22–27] characterized postsynaptic MT plus-end dynamics by performing particle tracking and analysis of green fluorescent protein (GFP)-tagged EB1. Such studies in Drosophila[22–27] and other systems[28–32] have significantly advanced understanding of single-polymer behavior of MT plus ends in the dendrites of developing neurons[33].

Despite the impressive in vivo studies of postsynaptic MT dynamics[22–31], there have been far fewer comparable studies of presynaptic MT dynamics at the developing axon terminal. MT dynamics at the Drosophila larval NMJ has been studied using fluorescent speckle microscopy (FSM) and fluorescence recovery after photobleaching (FRAP)[34]. These techniques evaluate the overall tubulin kinetics but not the behavior of individual MT plus ends. As of this writing, there has been one sole investigation of individual MT plus ends at the Drosophila NMJ: This study combined live time-lapse imaging with manual analysis of kymographs to characterize a population of dynamic, EB1-GFP labeled "pioneering MTs" that appeared distinct from a broader population of stabilized MTs[35]. This lack of research on presynaptic MT dynamics may be due at least in part to anatomy: While it is relatively straightforward to obtain images of dendrites due to their proximity to the larval cuticle, NMJs are obstructed by other tissues, making it challenging to acquire images with sufficient signal-to-noise ratio for particle-level analysis. Nonetheless, given the well-established importance of the presynaptic MTs to synaptic morphogenesis and stabilization[36], as well as their links to neurodevelopmental and neurodegenerative disorders[37], bridging this gap between understanding of pre- and postsynaptic MTs is likely to yield invaluable insights.

An additional challenge to the analysis of in vivo MT dynamics in general, in contrast to in vitro or ex vivo analysis, is the limited automated software tools that can extract dynamics parameters from in vivo data. Presently, one of the most popular and powerful techniques for analysis of +TIP-labeled MT plus ends is plusTipTracker[38,39], a MATLAB-based software that allows automated tracking and analysis of multiple dynamics parameters. Notably, plusTipTracker

measures not only MT growth but also shrinkage and rescues: while +TIP labels such as EB1-GFP only associate with growing plus ends, plusTipTracker can algorithmically infer shrinkage rates and rescue events. However, while plusTripTracker has been very successfully applied to many contexts, including previous multiparametric analysis of ex vivo MT dynamics in Drosophila S2 cells[40], plusTipTracker is not optimal for analysis of in vivo data given their lower signal-to-noise ratio. As a result, in vivo studies of plus-end dynamics at dendrites[22–27] and at the NMJ[35] of Drosophila have relied on manual generation and analysis of kymographs using software such as ImageJ[41], or on semiautomated strategies that involve numerous human-in-the-loop components.

This study presents an experimental and analytical workflow that reduces the experimental and analytical overhead required to perform noninvasive polymer-level analysis of presynaptic MT dynamics in both sensory dendrites and the motor axon terminal of Drosophila third-instar larvae. The protocol utilizes immobilized, intact larvae and therefore avoids injuries known to trigger stress responses as well as other nonphysiological conditions that might perturb in vivo MT dynamics. To label dynamic MT plus-ends, EB1-GFP is pan-neuronally expressed using the *Gal4/UAS* system[42], allowing visualization of MTs at both dendrites and NMJ with a single driver. While some early steps are inevitably subject to human decision-making, such as the selection of animal specimens and identification of regions to image, the steps following data acquisition are largely automated. Crucially, optimization of a new software enabled automated, unbiased analysis requiring minimal human input. While other particle tracking methods are available[43–45], this study utilizes a proprietary software because it was algorithmically well-suited to address the particular challenges of this particular dataset. The software is now available to users for a variety of applications. Specifically, the use of coherence-enhancing diffusion filtering[46] is integral to automated segmentation and background removal, and custom algorithms are implemented specifically to automate particle detection and tracking. This strategy could effectively handle the low signal-to-noise ratio inherent to the data in this study, as well as other challenges, such as movement of EB1-GFP comets through different focal planes. While it is not feasible to exhaustively test the performance of this software against all other particle analysis software, the performance of the present strategy equaled or approached the standard human performance. Furthermore, to the authors' knowledge, there has been no other software specifically trained on in vivo data from sensory dendrites and the presynaptic terminal. Given that the performance of image analysis algorithms is often highly specific to the data they were designed for and that generalized computer vision is not yet possible, it is expected that training the described software to the specific in vivo data of interest is the most algorithmically sound approach.

Given the extensive work on dendritic MTs[22–27] as well as the consistent quality of data that can be acquired from this system, the image acquisition and software analysis strategy was first validated in Drosophila sensory dendrites. Importantly, it was found in dendrites that the use of different neuronal *Gal4* drivers, even in otherwise identical wild type backgrounds, results in significant differences in EB1-GFP dynamics due to differences in genetic background, emphasizing the importance of using a single *Gal4* driver for consistent results. This strategy was next used for multiparametric analysis of EB1-GFP dynamics at the presynaptic terminal of the

NMJ. To further illustrate the investigative value of this method, this imaging and software strategy was used to assess both pre- and postsynaptic EB1-GFP dynamics following knockdown of dTACC, the Drosophila homolog of the highly conserved TACC (transforming acidic coiled coil) family[47,48]. Prior work in Drosophila S2 cells[40], as well as work by Lowery and colleagues in the Xenopus growth cone[49–51], has shown that TACC family members regulates MT plus-end dynamics. Furthermore, recently reported evidence from confocal and super-resolution immunofluorescence imaging showed that dTACC is a key regulator of presynaptic MTs during neuronal morphogenesis[52], raising the question of whether dTACC regulates live MT dynamics. This report demonstrates a method that can indeed detect differences in live MT behaviors upon dTACC knockdown. Thus, this study presents an in vivo method that can effectively identify and characterize key regulators of MT dynamics within the developing neuron, particularly in the presynaptic compartment.

PROTOCOL:

1. Generation of Drosophila specimens

1.1. Select a suitable MT plus-end marker. This study utilized GFP-tagged EB1, a well-characterized plus-end marker with a strong, clear signal[11,12]. Alternatives include other +TIPs such as EB3[10,13], CLASP/Orbit[53], and CLIP-170[54].

1.2. Obtain or generate flies with the MT marker under control of a UAS promoter (e.g., *UAS-EB1-GFP*).

1.3. Choose the appropriate tissue-specific *Gal4*-driver. This study used the pan-neuronal driver *elaV-Gal4*[58,59] to drive expression in both sensory dendrites and at the NMJ and *221-Gal4*[60,61] for dendrite-specific expression.

1.4. Raise flies using standard fly husbandry techniques[55,56]. It is recommended that flies be kept in humidified incubators at 25 °C for optimal *Gal4/UAS* expression.

1.5. Using standard fly genetic techniques[55,56], perform crosses to generate flies to express the MT plus-end marker in the desired cells/tissues.

NOTE: For any *Gal4*-driver and UAS-transgene combination, the experimental design should include proof-of-concept and validation experiments to characterize the system and avoid artifacts from overexpression.

2. Equipment setup

2.1. Set up a workstation, including the flies, anesthetic reagents, slide construction materials, stereomicroscope, and illumination source, close to the confocal microscope (i.e., in the same room) to minimize the time spent between sample preparation and imaging to prolong the health and viability of the larvae.

2.2. Prepare the anesthetic by mixing a 9% chloroform mixture (0.1 mL of chloroform and 1.0 mL of halocarbon oil) in a 1.5 mL microcentrifuge tube. To avoid separation, mix well by inverting the tube prior to preparing each new slide.

2.3. Prepare the glass slide: Cut four strips of double-sided tape (~15 mm wide). Line up two of the pieces on the glass slide, leaving a space of ~5 mm in between the strips. Layer the remaining two pieces on top of the first two to double the thickness of the tape (**Figure 1C**).

2.4. Add a large drop (~100 µL) of chloroform/oil mixture onto the glass slide in the 5 mm space between the tape pieces (**Figure 1C**).

3. Preparation of larval samples for imaging

3.1. Fill a container (e.g., a 6 well plate) with 1x PBS.

3.2. Collect 3rd instar larvae from the fly vial using forceps or a similar instrument. Identify larvae at the proper stage by their crawling behavior and by the presence of 9–12 prominent, serrated mouth hooks. Use a stereomicroscope to assist in staging larvae (**Figure 1D**).

3.3. Place a larva in the PBS and move it gently to wash off any remains of food or other debris. Dry the larva gently on a delicate tissue.

3.4. Anesthetize the larva by placing it into chloroform/oil drop on the slide from section 2 (**Figure 1C**).

NOTE: The dorsal/ventral orientation of the larva is not critical because both sensory and motor neurons can be detected through the translucent cuticle by setting the microscope stage to the proper focal plane, regardless of the orientation of the specimen.

3.5. Place a #1.5 coverslip on top. Adhere the coverslip to the tape by applying gentle pressure, thus immobilizing the larva without damaging it (**Figure 1C**).

3.6. Seal the chamber with petroleum jelly or nail polish.

4. Time-lapse confocal imaging of live samples

4.1. Prepare confocal microscope and the 60x objective lens with oil immersion. Place the sample on the stage (**Figure 1A**,**B**).

4.2. Use the acquisition software to configure experiments.

NOTE: For this study, each imaging series was acquired at a single focal plane as opposed to a z-stack.

4.2.1. Set the time-lapse duration to 30 s at an interval of 2 s, for a total of 16 frames.

4.2.2. Set laser exposure and intensity to ensure sufficient signal while avoiding saturation and photobleaching.

4.2.3. For EB1-GFP imaging, the 488 nm laser was set to an exposure time of 100 ms and intensity of 30%. These values may vary for different uses of this protocol and should be modified empirically.

4.3. Use the eyepieces of the microscope to find the larva in widefield-green illumination. Find the dendrites or NMJs by adjusting the stage slowly. Do not expose larva to illumination (widefield or confocal) for longer than necessary.

4.3.1. Dendrites appear as thin bright-green webs of nerves easily distinguishable from thick long axon bundles (**Figure 1E**).

4.3.2. NMJs appear as groups of bright-green individual boutons, approximately 5 µm in diameter, at the ends of thick long axon bundles that diverge from the nerve cord (**Figure 1F**).

4.4. Using the live camera feed, quickly focus on the region of interest using 488 nm illumination. Immediately stop illumination once the proper focus is found to avoid phototoxicity.

4.5. Initiate image acquisition. EB1 comets are recognizable as bright, motile punctae.

4.6. Refer to previously published protocols for additional details and guidelines on fluorescence live imaging[57].

5. Software-based image processing and analysis

5.1. Analyze each video file individually. Within software (user interface shown in **Figure 2**), select **File | Import | Image Sequence** and drag TIF files in the box that appears. Preview the video.

5.2. Under the **Detection Parameters** menu, tune the software parameters to ensure detection of only clearly visible punctae and avoid detection of spurious objects. For instance, reducing particle intensity results in greater sensitivity of software to punctae but increases potential false positives. The precise values of the parameters will vary empirically. Descriptions of the Detection and Tracking Parameters are available from the authors upon request.

5.3. Apply the **Neuron Particle Tracking** recipe to analyze the image using the **From beginning** button (blue arrow, **Figure 2B**). The software will output results for the tracking parameters listed in **Table 1** to the **Results Spreadsheet** (green box, **Figure 2B**). For ease of later analysis and

interpretation, the results can be stored in spreadsheet software using the **Export** function found in the **Results Spreadsheet** section.

5.4. Navigate the cursor to puncta detected in the previous step and **left-click** to select or deselect. Multiple puncta can be selected simultaneously using **Ctrl + left-click**.

NOTE: Depending on the project aims and applications, additional heuristics may be used to filter the punctae. For instance, punctae with a lifetime of fewer than 8–10 s (4–5 frames) might be omitted because they do not present sufficient information about the entire growth event. The need for such heuristics will vary empirically. Additional details on software functionality are available from the authors upon request.

REPRESENTATIVE RESULTS:

Flies were raised from stable stocks that constitutively express the UAS-EB1-GFP transgene either pan-neuronally (*elaV-Gal4; UAS-EB1-GFP*)[58,59] or in sensory neurons (*221-Gal4; UAS-EB1-GFP*)[60,61]. EB1 was chosen for this study because it specifically localizes to growing ends and dissociates immediately upon pause and shrinkage[14,15] and has been shown through multiple studies, including in Drosophila[22–27,35], to be a robust marker that does not have significant detrimental effects on the underlying biology of the organism. Imaging of wandering third-instar larvae was performed on an inverted spinning disc confocal microscope following the preparation of intact samples (**Figure 1A–C**). Larvae were staged based on behavior (active crawling along vial walls) and the presence of large, extended mouth hooks with 9–12 teeth (**Figure 1D**). Each image series was acquired at a single focal plane. Sensory dendrites superficially located near the larval cuticle (**Figure 1E**) were imaged to provide comparisons with published data[22–27,35], while NMJs located at deeper image planes on the surface of body wall muscle within the animal (**Figure 1F**) were imaged to define presynaptic MT dynamics parameters.

Following image acquisition as described in the protocol above automated, unbiased analysis of the EB1-GFP comets was performed (**Figure 2**), producing measurements for nine dynamic parameters (**Table 1**). Statistical analysis, including exploratory data analysis and hypothesis testing, was performed in MATLAB. It was noted through data visualization and the Anderson-Darling test that the data contained non-normally distributed values. Thus, to avoid making assumptions about the underlying distribution of the data, all hypothesis testing was performed using the nonparametric Wilcoxon-Mann-Whitney test.

EB1-GFP dynamics under the control of both the *elaV-Gal4* and *221-Gal4* drivers were compared in otherwise equivalent wild type backgrounds (**Figure 3**). Interestingly, there were highly significant differences ($P < 0.005$) in several measured parameters (e.g., mean acceleration, sinuosity, growth length). While EB1 is not generally expected to disrupt native MT biology to an adverse degree[10,54], MTs are nevertheless highly sensitive to perturbations in EB1 expression[62,63]. The differences observed between the two drivers could arise from their distinct expression patterns: *elaV-Gal4* could drive *UAS-EB1-GFP* expression pan-neuronally as well as in neuronal progenitors and glia[58,59] while *221-Gal4* could drive expression solely in sensory dendrites[60,61]. Differences in *UAS-EB1-GFP* expression could also be due to different temporal onset of *elaV-*

Gal4 and *221-Gal4,* or any number of other variations in the genetic background of the two driver lines. To avoid any artifacts from these and other potentially confounding factors, all further experiments in both dendrites and at the NMJ were carried out using only the *elaV-Gal4* pan-neuronal driver.

This method was first validated in sensory dendrites (**Figure 4**), and the entire protocol was repeated at the NMJ (**Figure 5**). To assess the potential of this strategy for investigating the role of specific molecules on MT dynamics, EB1-GFP dynamics were compared between wild type controls and animals expressing *UAS-dtacc-RNAi*. dTACC was chosen because it is a known regulator of MT plus-end dynamics[40,49–51] in other systems, and also based on recent evidence that it regulates presynaptic MTs at the *Drosophila* NMJ[52]. To enhance *dtacc-RNAi* expression, *elaV*-GAL4 was also used to express *UAS-Dcr2*, an endonuclease that promotes processing of long dsRNAs to siRNAs.

Upon reduction of dTACC expression to ~50%[52], significant changes in EB1-GFP dynamics were found in both dendrites (**Figure 4**) and at the NMJ (**Figure 5**). Notably, the effects of dTACC knockdown in dendrites closely resembled the effects of dTACC knockdown previously observed in S2 cells[40]. In contrast, striking differences were observed between dendrites and the NMJ upon dTACC knockdown. While loss of dTACC affected seven parameters in dendrites, and three parameters at the NMJ, all but two of the parameters (max comet velocity and sinuosity) were unique to either dendrites or NMJ. Furthermore, while sinuosity was affected by dTACC loss in both contexts, the effect was opposite between dendrites (increase) and the NMJ (decrease). Thus, this protocol can not only identify significant differences in MT dynamics between genetic backgrounds but can also demonstrate distinct roles for a single MT regulator in different contexts.

FIGURE AND TABLE LEGENDS:

Figure 1: Experimental setup. (**A**) Schematic and (**B**) actual example of imaging setup. Anesthetized, whole-mount larvae were imaged on an inverted spinning disc confocal microscope. (**C**) Example of slide preparation using third-instar larvae. (**D**) Larvae were staged by their crawling behavior and by the presence of 9–12 prominent, serrated mouth hooks. Imaging was performed on (**E**) sensory neuron dendrites, which have a relatively superficial location close to the outer cuticle, and (**F**) the presynaptic terminal of the NMJ, which is located deeper within the animal. Scale bar = 2 μm.

Figure 2: Demonstration of software-based dendrite and NMJ analysis. (**A**) Summary of the automated analysis processing pipeline. A common issue of typical morphological approaches to background removal is the enhancement of image signal along the edges of small and narrow structures (e.g., dendrites). To address this, a coherence-enhancing diffusion filter[46] was applied to the raw image to extract the whole dendrite/NMJ structure as background and to isolate the EB1 comets on the image. This approach enabled identification and tracking of the comets even where the contrast between the background structure and the EB1 comet was low. (**B**) Workflow integration by the software interface allows the user to 1) optimize analysis parameters for a given image, and 2) review the analysis. The blue arrow highlights the button used to run the

recipe, and the green box indicates the spreadsheet with analysis results. Additional details on software functionality are available from the authors upon request.

Figure 3: Comparison of *elaV*- and *221-Gal4* drivers in wild type control dendrites. To determine the effects of Gal4-dependent *UAS-EB1-GFP* expression levels on EB1-GFP dynamics, *elaV-Gal4; UAS-EB1-GFP* and *221-Gal4; UAS-EB1-GFP* were expressed in a w^{1118} control background. Highly significant differences were observed in mean acceleration, sinuosity, and growth length. ** P < 0.005, Wilcoxon-Mann-Whitney-test; error bars indicate ± SEM; number of NMJs quantified indicated on graph.

Figure 4: Neuronal RNAi-knockdown of TACC affected EB1-GFP dynamics in sensory dendrites. (**A**) Representative time-lapse images of EB1-GFP comet dynamics in control *elaV-Gal4; UAS-EB1-GFP; UAS-Dcr2* x w^{1118} sensory dendrites. Image series on the right shows a detailed view of the region indicated by the box in the image on the left. In each panel, the solid white arrow indicates the position of the EB1-GFP comet at the most recent timepoint, while the hollow arrow indicates the original position of the comet at t = 0 s. (**B**) Comparison of EB1-GFP dynamics in *elaV-Gal4;UAS-EB1-GFP; UAS-Dcr2* x w^{1118} and *elaV-Gal4; UAS-EB1-GFP; UAS-Dcr2* x *UAS-tacc-rnai* dendrites. Knockdown of dTACC significantly affected all dynamics parameters other than mean acceleration and growth lifetime. * P < 0.05, ** P < 0.005, Wilcoxon-Mann-Whitney-test; error bars indicate ± SEM; number of NMJs quantified indicated on graph; scale bar = 1 µm.

Figure 5: Neuronal RNAi-knockdown of TACC affected EB1-GFP dynamics at the NMJ. (**A**) Representative time-lapse images of EB1-GFP comet dynamics at the presynaptic terminal of control *elaV-Gal4; UAS-EB1-GFP; UAS-Dcr2* x w^{1118} NMJs. Image series on the right shows detailed view of the region indicated by the box in the image on the left. In each panel, the solid white arrow indicates the position of the EB1-GFP comet at the most recent timepoint, while the hollow arrow indicates the original position of the comet at t = 0 s. (**B**) Comparison of EB1-GFP dynamics at *elaV-Gal4; UAS-EB1-GFP; UAS-Dcr2* x w^{1118} and *elaV-Gal4; UAS-EB1-GFP; UAS-Dcr2* x *UAS-tacc-rnai* NMJs. Knockdown of dTACC significantly affected max velocity, mean acceleration, and sinuosity. * P < 0.05, ** P < 0.005, Wilcoxon-Mann-Whitney-test; error bars indicate ± SEM; number of NMJs quantified indicated on graph; scale bar = 1 µm.

Table 1: Plus-end dynamic parameters analyzed

DISCUSSION:

This paper discusses a protocol to perform noninvasive intravital imaging of MT dynamics in the dendrites and at the NMJ of Drosophila during development. Human input is required during the experimental steps, such as in selecting animals to image, and may introduce bias in the data collection process that cannot be reasonably removed. Thus, a key goal of the protocol is to minimize bias wherever possible by performing automated analysis with a new software (section 5) that was optimized to handle the low signal-to-noise ratio inherent to in vivo imaging data. Importantly, the algorithms used in this study allow machine-based particle detection, kymograph generation, and track analysis, reducing the need for human input compared to traditional methods. Regardless, users of the software should assess the results and set the

tracking and detection parameters to filter out false positives (e.g., aggregates or noise). These modifications must be empirically adjusted based on each user's unique data and use. It is also worth noting that the analysis presented here is not completely equivalent to that possible with plusTipTracker: While it is possible to infer shrinkage and rescue events with plusTipTracker, the algorithms in the current software cannot perform such measurements. Furthermore, because each imaging series is acquired at a single focal plane, movement of EB1 comets in the z axis cannot be fully captured using the current protocol. Nonetheless, despite these limitations, given the considerable constraints on data quality that are inherent to in vivo data, this method makes progress towards achieving automated, reproducible data analysis in vivo.

Because the quality of the raw data is also paramount regardless of the capabilities of the analysis software, optimal specimen preparation is also a critical consideration. While every effort must be made to reduce deleterious effects on the larva (e.g., using intact samples), stresses such as chloroform and phototoxicity are inevitable. Thus, care should be made when setting imaging parameters to ensure specimen health, based both on general guidelines[57] and empirical monitoring. It was found that expediting the experimental steps by working quickly and having a sample preparation workstation in the same room as the confocal microscope (section 2) helped to mitigate sample deterioration and prolong larval viability. Another key aspect of the method is to find a chloroform dosage that is sufficiently potent but not overly harmful. Nevertheless, it should be noted that general anesthetization may influence MT dynamics[64]. The use of nonchemical methods of immobilizing larvae, such as adhering larvae to an agarose pad[25] or microfluidic chambers[65,66], may further improve results by circumventing the potential side effects of anesthetization.

Another crucial step is the method by which EB1-GFP is expressed using the *Gal4/UAS* system to label MT dynamics (section 1). As already noted, it is imperative to maintain a consistent genetic background throughout all comparisons due to the potential for multiple confounding variables that can influence EB1-GFP dynamics (**Figure 3**). A further consideration when using *Gal4/UAS* or other similar targeted expression systems is the effect of overexpression on endogenous MT dynamics. Thus, a possible future improvement would be to utilize knock-in fluorescent tags to avoid gain-of-function artifacts, although at present, *Gal4/UAS* remains a very widely used method in studies of live MT dynamics in Drosophila[22–27,35]. An issue regarding the use of fluorescently-tagged +TIPs to keep in mind is the potential ectopic effect of the tag on +TIP function. Thus, any novel fusion constructs should be validated through rescue experiments, and data analysis and interpretation should be performed with these points in mind.

Significant effects on multiple MT dynamics parameters were observed upon knockdown of dTACC in both dendrites and at the NMJ. This demonstrates that this method may be a potential screening tool for regulators of synaptic MT dynamics and moreover identifies a potential role for dTACC in dendrites. While the role of presynaptic dTACC in the development of the motor axon terminal has been established[52], the roles of postsynaptic dTACC are unknown. Thus, future studies may focus on role of postsynaptic dTACC, either in sensory dendrites and/or in the muscle of the NMJ.

Key differences were noted in the effects of dTACC knockdown on MT dynamics in sensory dendrites and the NMJ, indicating clear biological differences between the two contexts. This raises the question of whether MT dynamics differs between neuronal types, between distinct compartments of a single neuron, or both. The differences observed between dendrites and the NMJ might reflect differences between sensory and motor neurons but could also indicate differences between dendritic and axonal compartments, independent of the neuronal type. Because the focus in the present study was on developing a robust methodology rather than comprehensive characterization of neuronal MT dynamics, analysis of motor neuron dendrites or the axon terminals of sensory neurons has not yet been performed. Due to their less accessible location within the animal, these structures are more challenging to image and analyze compared to the structures presently discussed. Future efforts will focus on applying this optimized protocol to improve imaging of less accessible regions to enable studies of compartment- and cell-type differences in MT dynamics.

Conceivably, this in vivo imaging and analysis strategy will be of value to researchers interested in a detailed understanding of the dynamic MT behaviors during the critical stages of neuronal development. A key future innovation would be multicolor imaging through coexpression of EB1-GFP with other markers, such as those that label the cell membrane (i.e., CD8[67], myristol[68]), the actin cytoskeleton (i.e., moesin[69], LifeAct[70]), and other structures of interest. This would allow correlative analysis of the spatiotemporal interactions of MTs with other key cellular structures. While such multicolor imaging has been used to study MT-actin interactions in the neuronal growth cone[71,72], it has not been employed in dendrites or the presynaptic axon terminal. Thus, developing a comparable method for in vivo Drosophila studies will be a significant addition to the imaging toolkit for understanding the role of MTs in the broader context of neuronal development.

ACKNOWLEDGMENTS:

We thank our colleagues in the Van Vactor lab and at DRVision in addition to Drs. Max Heiman, Pascal Kaeser, David Pellman, and Thomas Schwarz for helpful discussion. We thank Dr. Melissa Rolls for generously providing the *elaV-Gal4; UAS-EB1-GFP; UAS-Dcr2* and *221-Gal4; UAS-EB1-GFP* stocks used in this study. We thank Drs. Jennifer Waters and Anna Jost at the Nikon Imaging Center at Harvard for light microscopy expertise. This work is funded by the National Institutes of Health (F31 NS101756-03 to V.T.C., SBIR 1R43MH100780-01D to J.S.L.).

DISCLOSURES:

The authors Hoyin Lai, Michael Jones, Hideki Sasaki, Luciano A.G. Lucas, Sam Alworth (formerly), and James Shih-Jong Lee are employees of DRVision Technologies LLC, which produces the software used in this protocol.

REFERENCES:

1. Rolls, M. M. Neuronal polarity in Drosophila: Sorting out axons and dendrites. *Developmental Neurobiology.* **71** (6), 419–429 (2011).
2. Jan, Y. N., Jan, L. Y. Branching out: Mechanisms of dendritic arborization. *Nature Reviews Neuroscience.* **11** (5), 316–328 (2010).

3. Lewis, T. L., Courchet, J., Polleux, F. Cell biology in neuroscience: Cellular and molecular mechanisms underlying axon formation, growth, and branching. *Journal of Cell Biology.* **202** (6), 837–48 (2013).
4. Kandel, E. R. The Molecular Biology of Memory Storage: A Dialogue Between Genes and Synapses. *Science.* **294** (5544), 1030–1038 (2001).
5. Turney, S. G., Lichtman, J. W. Chapter 11: Imaging Fluorescent Mice In Vivo Using Confocal Microscopy. *Methods in Cell Biology*. **89** (8), 309–327 (2008).
6. McCann, C. M., Lichtman, J. W. In vivo imaging of presynaptic terminals and postsynaptic sites in the mouse submandibular ganglion. *Developmental Neurobiology.* **68** (6), 760–770 (2008).
7. Turney, S. G., Walsh, M. K., Lichtman, J. W. In vivo imaging of the developing neuromuscular junction in neonatal mice. *Cold Spring Harbor Protocols.* **7** (11), 1166–1176 (2012).
8. Tanaka, E., Ho, T., Kirschner, M. W. The role of microtubule dynamics in growth cone motility and axonal growth. *Journal of Cell Biology.* **128** (1-2), 139–155 (1995).
9. Tanaka, E. M., Kirschner, M. W. Microtubule behavior in the growth cones of living neurons during axon elongation. *Journal of Cell Biology.* **115** (2), 345–363 (1991).
10. Stepanova, T. et al. Visualization of microtubule growth in cultured neurons via the use of EB3-GFP (end-binding protein 3-green fluorescent protein). *Journal of Neuroscience.* **23** (7), 2655–2664 (2003).
11. Tirnauer, J. S., Bierer, B. E. EB1 proteins regulate microtubule dynamics, cell polarity, and chromosome stability. *Journal of Cell Biology.* **149** (4), 761–766 (2000).
12. Schwartz, K., Richards, K., Botstein, D. BIM1 encodes a microtubule-binding protein in yeast. *Molecular Biology of the Cell.* **8** (12), 2677–2691 (1997).
13. Juwana, J. P. et al. EB/RP gene family encodes tubulin binding proteins. *International Journal of Cancer* **81** (2) 275–284 (1999).
14. Akhmanova, A., Steinmetz, M. O. Tracking the ends: a dynamic protein network controls the fate of microtubule tips. *Nature Reviews Molecular Cell Biology.* **9** (4), 309–322 (2008).
15. Akhmanova, A., Steinmetz, M. O. Control of microtubule organization and dynamics: Two ends in the limelight. *Nature Reviews Molecular Cell Biology.* **16** (12), 711–726 (2015).
16. Mitchison, T., Kirschner, M. Dynamic Instability of microtubule growth. *Nature* **312** (15), 237–242 (1984).
17. Van De Willige, D., Hoogenraad, C. C., Akhmanova, A. Microtubule plus-end tracking proteins in neuronal development. *Cellular and Molecular Life Sciences.* **73** (10), 2053–2077 (2016).
18. Rebollo, E., Karkali, K., Mangione, F., Martín-Blanco, E. Live imaging in Drosophila: The optical and genetic toolkits. *Methods*. **68** (1), 48–59 (2014).
19. Bier, E. Drosophila, the golden bug, emerges as a tool for human genetics. *Nature Reviews Genetics.* **6** (1) 9–23 (2005).
20. Zito, K., Parnas, D., Fetter, R. D., Isacoff, E. Y., Goodman, C. S. Watching a synapse grow: noninvasive confocal imaging of synaptic growth in Drosophila. *Neuron*. **22** (4), 719–729 (1999).
21. Miller, K. E. et al. Direct observation demonstrates that Liprin-alpha is required for trafficking of synaptic vesicles. *Current Biology.* **15** (7), 684–689 (2005).

22. Rao, K. et al. Spastin, atlastin, and ER relocalization are involved in axon but not dendrite regeneration. *Molecular Biology of the Cell.* **27** (21), 3245–3256 (2016).
23. Hill, S. E. et al. Development of dendrite polarity in Drosophila neurons. *Neural Development.* **7**, 34 (2012).
24. Stone, M. C., Nguyen, M. M., Tao, J., Allender, D. L., Rolls, M. M. Global up-regulation of microtubule dynamics and polarity reversal during regeneration of an axon from a dendrite. *Molecular Biology of the Cell.* **21** (5), 767–777 (2010).
25. Mattie, F. J. et al. Directed microtubule growth, +TIPs, and kinesin-2 are required for uniform microtubule polarity in dendrites. *Current Biology.* **20** (24), 2169–2177 (2010).
26. Stone, M. C., Roegiers, F., Rolls, M. M. Microtubules Have Opposite Orientation in Axons and Dendrites of Drosophila Neurons. *Molecular Biology of the Cell.* **19** (10), 4122–4129 (2008).
27. Rolls, M. M. et al. Polarity and intracellular compartmentalization of Drosophila neurons. *Neural Development.* **2**, 7 (2007).
28. Hu, X., Viesselmann, C., Nam, S., Merriam, E., Dent, E. W. Activity-dependent dynamic microtubule invasion of dendritic spines. *Journal of Neuroscience.* **28** (49), 13094–13105 (2008).
29. Merriam, E. B. et al. Dynamic microtubules promote synaptic NMDA receptor-dependent spine enlargement. *PLoS One* **6** (11), e27688 (2011).
30. Hu, X. et al. BDNF-induced increase of PSD-95 in dendritic spines requires dynamic microtubule invasions. *Journal of Neuroscience.* **31** (43), 15597–15603 (2011).
31. Merriam, E. B. et al. Synaptic regulation of microtubule dynamics in dendritic spines by calcium, F-actin, and drebrin. *Journal of Neuroscience.* **33** (42), 16471–16482 (2013).
32. Jaworski, J. et al. Dynamic Microtubules Regulate Dendritic Spine Morphology and Synaptic Plasticity. *Neuron* **61** (1), 85–100 (2009).
33. Dent, E. W. Of microtubules and memory: Implications for microtubule dynamics in dendrites and spines. *Molecular Biology of the Cell.* **28** (1), 1–8 (2017).
34. Yan, Y., Broadie, K. In vivo assay of presynaptic microtubule cytoskeleton dynamics in Drosophila. *Journal of Neuroscience Methods* **162** (1-2), 198–205 (2007).
35. Pawson, C., Eaton, B. A., Davis, G. W. Formin-dependent synaptic growth: evidence that Dlar signals via Diaphanous to modulate synaptic actin and dynamic pioneer microtubules. *Journal of Neuroscience.* **28** (44), 11111–11123 (2008).
36. Ruiz-Cañada, C., Budnik, V. Synaptic cytoskeleton at the neuromuscular junction. *International Review of Neurobiology.* **75** (6), 217–236 (2006).
37. Bodaleo, F. J., Gonzalez-Billault, C. The presynaptic microtubule cytoskeleton in physiological and pathological conditions: lessons from Drosophila Fragile X syndrome and hereditary spastic paraplegias. *Frontiers in Molecular Neuroscience.* **9**, 60 (2016).
38. Applegate, K. T. et al. PlusTipTracker: Quantitative image analysis software for the measurement of microtubule dynamics. *Journal of Structural Biology.* **176** (2), 168–184 (2011).
39. Matov, A. et al. Analysis of microtubule dynamic instability using a plus-end growth marker. *Nature Methods*. **7** (9), 761–768 (2010).
40. Long, J. B. et al. Multiparametric analysis of CLASP-interacting protein functions during interphase microtubule dynamics. *Molecular and Cellular Biology.* **33** (8), 1528–1545

(2013).
41. Schneider, C. A., Rasband, W. S., Eliceiri, K. W. NIH Image to ImageJ: 25 years of image analysis. *Nature Methods*. **9** (7), 671–675 (2012).
42. Brand, A. H., Perrimon, N. Targeted gene expression as a means of altering cell fates and generating dominant phenotypes. *Development*. **118** (2), 401–415 (1993).
43. Ma, Y., Wang, X., Liu, H., Wei, L., Xiao, L. Recent advances in optical microscopic methods for single-particle tracking in biological samples. *Analytical and Bioanalytical Chemistry.* **411** (19), 4445–4463 (2019).
44. Shen, H. et al. Single Particle Tracking: From Theory to Biophysical Applications. *Chemical Reviews.* **117** (11), 7331–7376 (2017).
45. Zwetsloot, A. J., Tut, G., Straube, A. Measuring microtubule dynamics. *Essays in Biochemistry.* **62** (6), 725–735 (2018).
46. Weickert, J. Coherence-Enhancing Diffusion Filtering. *International Journal of Computer Vision.* **31** (2-3), 111–127 (1999).
47. Peset, I., Vernos, I. The TACC proteins: TACC-ling microtubule dynamics and centrosome function. *Trends in Cell Biology.* **18** (8), 379–88 (2008).
48. Hood, F. E., Royle, S. J. Pulling it together. *Bioarchitecture*. **1** (3), 105–109 (2011).
49. Lucaj, C. M. et al. Xenopus TACC1 is a microtubule plus-end tracking protein that can regulate microtubule dynamics during embryonic development. *Cytoskeleton.* **72** (5), 225–234 (2015).
50. Nwagbara, B. U. et al. TACC3 is a microtubule plus end-tracking protein that promotes axon elongation and also regulates microtubule plus end dynamics in multiple embryonic cell types. *Molecular Biology of the Cell.* **25** (21), 3350–3362 (2014).
51. Rutherford, E. L. et al. Xenopus TACC2 is a microtubule plus end–tracking protein that can promote microtubule polymerization during embryonic development. *Molecular Biology of the Cell.* **27** (20), 3013–3020 (2016).
52. Chou, V. T., Johnson, S., Long, J., Vounatsos, M. dTACC restricts bouton addition and regulates microtubule organization at the Drosophila neuromuscular junction. *Cytoskeleton.* **77** (1-2), 4–15 (2019).
53. Maiato, H. et al. Human CLASP1 Is an Outer Kinetochore Component that Regulates Spindle Microtubule Dynamics. *Cell.* **113** (7), 891–904 (2003).
54. Komarova, Y. A., Vorobjev, I. A., Borisy, G. G. Life cycle of MTs : persistent growth in the cell interior , asymmetric transition frequencies and effects of the cell boundary. *Journal of Cell Science.* **115** (Pt 17), 3527-3539 (2002).
55. Greenspan, R. J. *Fly pushing: The theory and practice of Drosophila genetics*. Cold Spring Harbor Laboratory Press (2004).
56. Hales, K. G., Korey, C. A., Larracuente, A. M., Roberts, D. M. Genetics on the fly: A primer on the drosophila model system. *Genetics*. **201** (3), 815–842 (2015).
57. Waters, J. C. *Live-cell fluorescence imaging*. *Methods in Cell Biology*. **114**, 125-150.
58. Berger, C., Renner, S., Lüer, K., Technau, G. M. The commonly used marker ELAV is transiently expressed in neuroblasts and glial cells in the Drosophila embryonic CNS. *Developmental Dynamics.* **236** (12), 3562–3568 (2007).
59. Robinow, S., White, K. Characterization and spatial distribution of the ELAV protein during Drosophila melanogaster development. *Journal of Neurobiology.* **22** (5), 443–461 (1991).

60. Parrish, J. Z., Kim, M. D., Lily, Y. J., Yuh, N. J. Genome-wide analyses identify transcription factors required for proper morphogenesis of Drosophila sensory neuron dendrites. *Genes and Development.* **20** (7), 820–835 (2006).
61. Grueber, W. B., Jan, L. Y., Jan, Y. N. Different levels of the homeodomain protein cut regulate distinct dendrite branching patterns of Drosophila multidendritic neurons. *Cell*. **112** (6), 805–818 (2003).
62. Zhang, T. et al. Microtubule plus-end binding protein EB1 is necessary for muscle cell differentiation, elongation and fusion. *Journal of Cell Science.* **122** (9), 1401–1409 (2009).
63. Yang, C. et al. EB1 and EB3 regulate microtubule minus end organization and Golgi morphology. *Journal of Cell Biology.* **216** (10) 3179–3198 (2017).
64. Allison, A., Nunn, J. Effect of general anaesthetics on microtubules. *Lancet*. **292** (7582), 1326–1329 (1968).
65. Mondal, S., Ahlawat, S., Koushika, S. P. Simple microfluidic devices for in vivo imaging of C. elegans, drosophila and zebrafish. *Journal of Visualized Experiments.* (67), e3780 (2012).
66. Mishra, B. et al. Using microfluidics chips for live imaging and study of injury responses in Drosophila larvae. *Journal of Visualized Experiments.* (84), e50998 (2014).
67. Lee, T., Luo, L. Mosaic analysis with a repressible neurotechnique cell marker for studies of gene function in neuronal morphogenesis. *Neuron*. **22** (5), 451–461 (1999).
68. Resh, M. D. Fatty acylation of proteins: New insights into membrane targeting of myristoylated and palmitoylated proteins. *Biochimica et Biophysica Acta.* **1451** (1), 1–16 (1999).
69. Edwards, K. A., Demsky, M., Montague, R. A., Weymouth, N., Kiehart, D. P. GFP-moesin illuminates actin cytoskeleton dynamics in living tissue and demonstrates cell shape changes during morphogenesis in Drosophila. *Developmental Biology.* **191** (1), 103–117 (1997).
70. Riedl, J. et al. Lifeact : a versatile marker to visualize F-actin. *Nature Methods*. **5** (7), 605–607 (2008).
71. Dent, E. W., Kalil, K. Axon Branching Requires Interactions between Dynamic Microtubules and Actin Filaments. *Journal of Neuroscience*. **21** (24), 9757–9769 (2001).
72. Schaefer, A. W., Kabir, N., Forscher, P. Filopodia and actin arcs guide the assembly and transport of two populations of microtubules with unique dynamic parameters in neuronal growth cones. *Journal of Cell Biology.* **158** (1), 139–152 (2002).

Figure

Click here to access/download;Figure;Figure1.psd

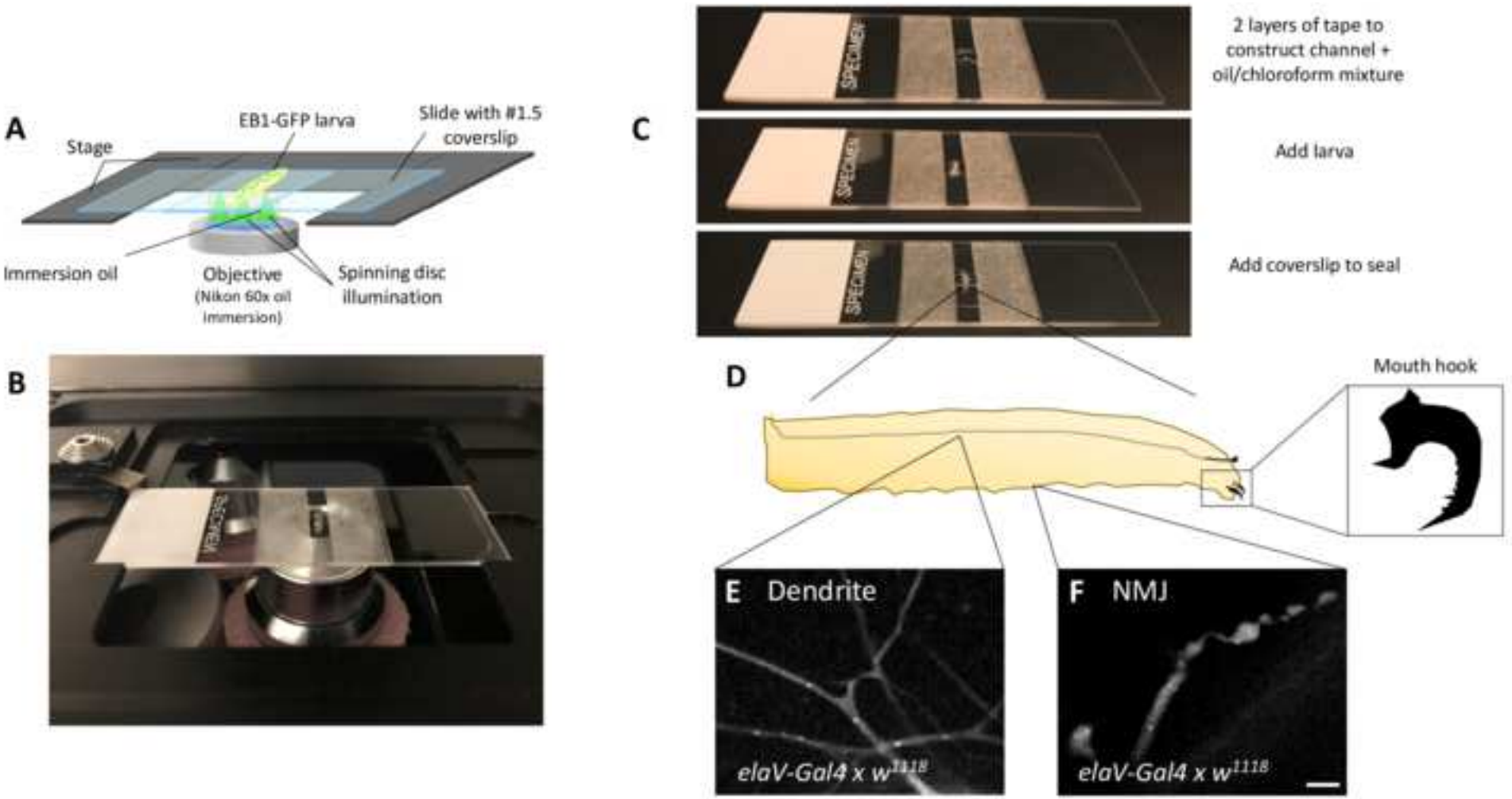

Figure

Click here to access/download;Figure;Figure2.psd

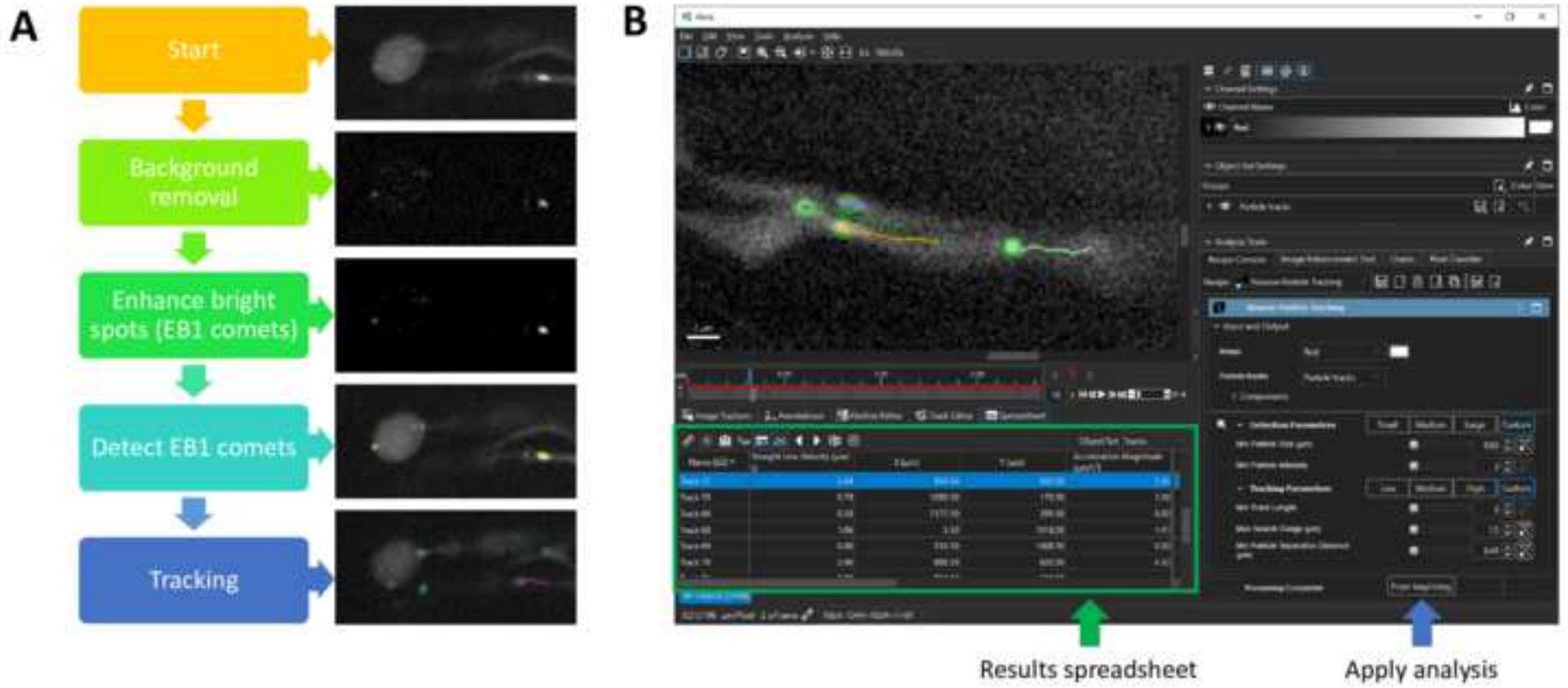

Figure

Click here to access/download;Figure;Figure3.psd

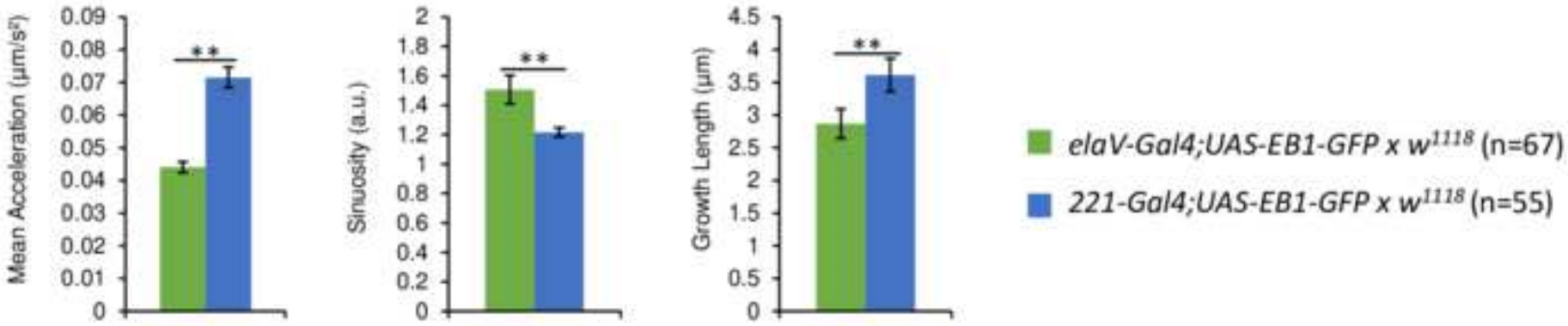

Figure 4

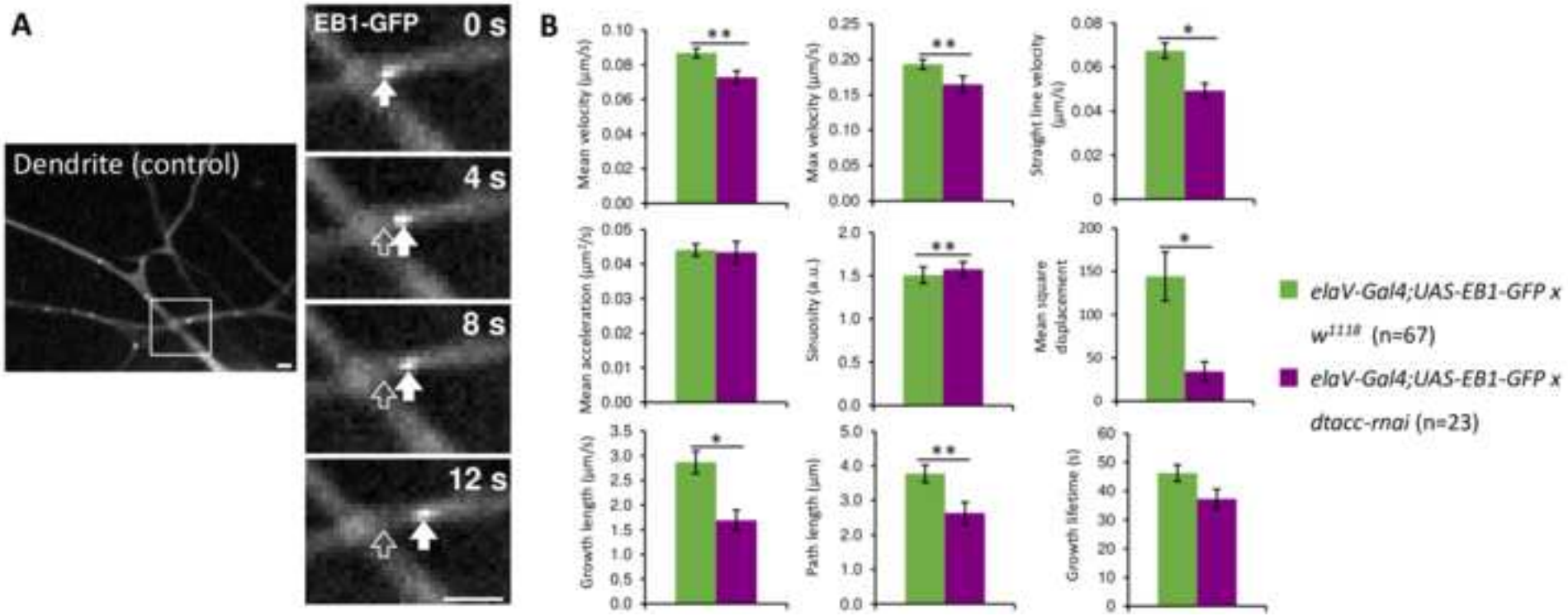

Figure 5

Click here to access/download;Figure;Vivian Chou - Figure5_rev.psd

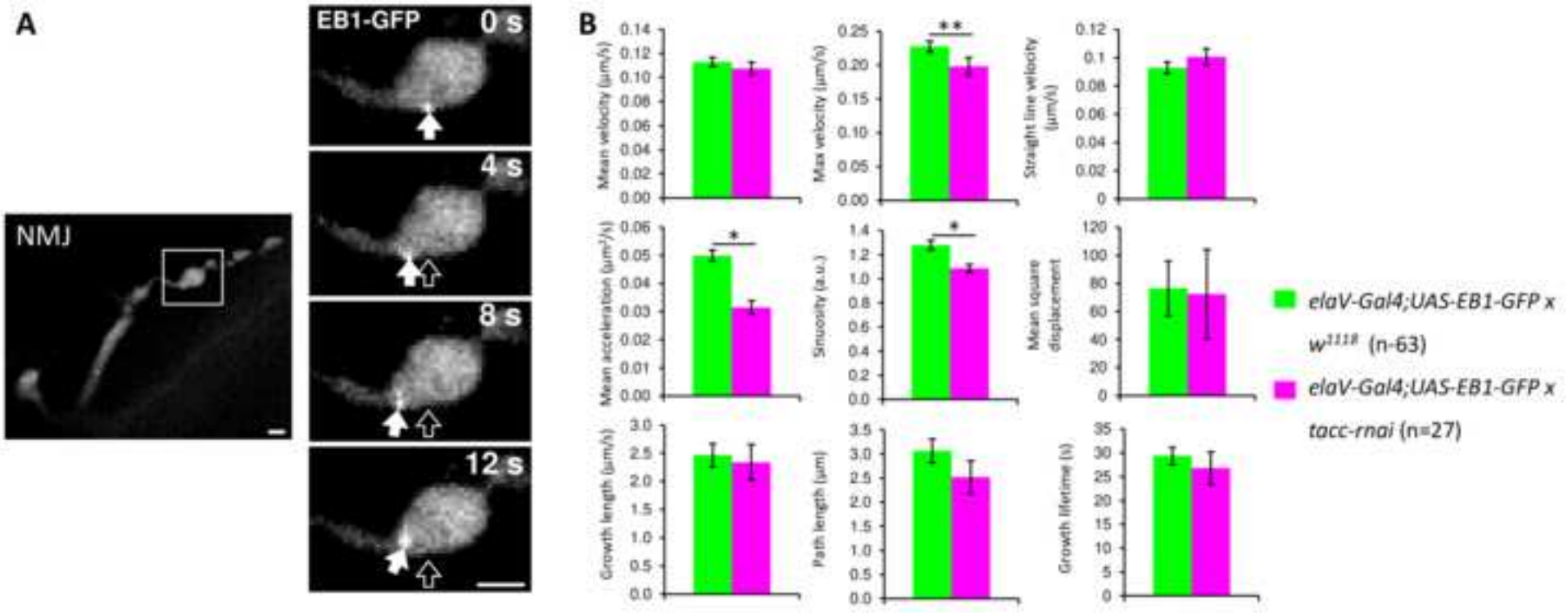

Tracking Parameter
Mean Comet Velocity
Max Comet Velocity
Straight Line Velocity
Mean Acceleration
Sinuosity
Mean Square Displacement
Growth Length
Path Length
Growth Lifetime

Description
average of the detected track velocity (scalar) over the lifetime of the track
highest value of track velocity (scalar) detected over the lifetime of the track
growth length divided by the growth lifetime
average of the rate of change of detected track velocity (scalar) over the lifetime of the track
growth length divided by path length
sum of the particle displacement squared at all time points divided by growth lifetime
straight line distance between the starting frame position and ending frame position of the track
total distance traveled by the track
total length (in time) of the detected track

Table of Materials

Click here to access/download;Table of Materials;Chou_etal_EB1tracking_materials_1.xlsx

Name of Material/Equipment	Company
1.5 mL microcentrifuge tube	Eppendorf
1000 µL TipOne pipette tips	USA Scientific
200 µL TipOne pipette tips	USA Scientific
221-Gal4 flies	Bloomington *Drosophila* Stock Center (US)
60x Objective Lens	Nikon
6-well plate	BD Falcon
Agar	MoorAgar
Aivia	DRVision LLC
Chloroform (stabilized with amylenes)	Sigma-Aldrich
CO2 blowgun (for selection of flies for crosses)	Genesee
CO2 bubbler (for selection of flies for crosses)	Genesee
Cooled CCD camera	Hamamatsu
Cornmeal	Genesee
Distilled Water	
Double-sided tape	Scotch
Drosophila vials	Genesee
Droso-plugs (foam plugs for vials)	Genesee
Dumont #5 Biologie Inox Forceps	Fine Science Tools
elaV-Gal4;UAS-EB1-GFP;UAS-Dcr2 flies	Gift of Melissa Rolls (Penn State University)
Ethanol (95%)	VWR
Fiber optic illuminator/light source for stereomicroscope	Nikon
Flypad (for selection of flies for crosses)	Genesee
Forma Environmental Chamber/Incubator	ThermoFisher
Halocarbon oil 700	Sigma-Aldrich
Immersion Oil	Nikon
Kimwipe Delicate Wipes	Fisher Scientific
Laser Merge Module	Spectral Applied Research
Light Source for Confocal	Lumencor
MetaMorph Microscopy Automation & Image Analysis Software	Molecular Devices
Micro Cover Glasses, Square, No. 1 1/2 (#1.5)	VWR
Motorized inverted microscope with Perfect Focus System	Nikon

Motorized stage and shutters	Prior
Multi-purpose scissors	Scotch
Nail Polish	Sally Hansen
Optical Filter	Chroma
P1000 Pipetman	Gilson
P200 Pipetman	Gilson
PBS (10X) ph 7.4	ThermoFisher
Propionic Acid	Fisher
Spinning disk confocal scanner unit	Yokagawa
Stereomicroscope	Nikon
Sugar (Sucrose)	Genesee
Superfrost Slide	VWR
Tegosept	Genesee
UAS-dtacc-RNAi flies	Vienna *Drosophila* Resource Center (Vienna, Austria
Vaseline petroleum jelly	WB Mason
Winsor & Newton Brush Regency Gold 520, Size 0	Staples
Yeast	VWR
Yokogawa dichroic beamsplitter	Semrock

Catalog Number	Comments/Description
21008-959	Sample preparation
1111-2721	Sample preparation
1120-8710	Sample preparation
26259	*Drosophila* genetics/crosses
Plan Apo 60x Oil	Image acquisition
353224	Sample preparation
41084	*Drosophila* food
	Optimized as part of this study
C2432	Sample preparation
54-104	*Drosophila* genetics/crosses
59-180	*Drosophila* genetics/crosses
ORCA-R2	Image acquisition
62-101	*Drosophila* food
	Drosophila food
	Sample preparation
32-109	*Drosophila* food
59-200	*Drosophila* food
11252-20	Sample preparation
N/A	*Drosophila* genetics/crosses
75811-022	*Drosophila* food
NI-150	Sample preparation
59-172	*Drosophila* genetics/crosses
3940	*Drosophila* genetics/crosses
H8898	Sample preparation
MXA22168	Image acquisition
34120	Sample preparation
LMM-5	Image acquisition
SOLA 54-10021	Image acquisition
	Image acquisition
48366-205	Sample preparation
TI-ND6-PFS-S	Image acquisition

Proscan III		Image acquisition
MMM1428		Sample preparation
784179032016 074170382839		Sample preparation
ET480/40m		Image acquisition
F123602		Sample preparation
F123601		Sample preparation
	70011044	Sample preparation
A258-500		*Drosophila* food
CSU-X1		Image acquisition
SMZ800N		Sample preparation
62-112		*Drosophila* food
48311-600		Sample preparation
20-258		*Drosophila* food
VDRC-101439		*Drosophila* genetics/crosses
DVOCB311003		Sample preparation
	5012000	*Drosophila* genetics/crosses
Torula Yeast IC90308580		*Drosophila* food
Di01-T405/488/568/647-13x15x0.5		Image acquisition

Compatibility Report for EB1_JoVE_Materials.xls
Run on 10/30/2019 10:18

If the workbook is saved in an earlier file format or opened in an earlier version of Microsoft Excel, the listed features will not be available.

Minor loss of fidelity	# of occurrences	Version
Some cells or styles in this workbook contain formatting that is not supported by the selected file format. These formats will be converted to the closest format available.	2	Excel 97-2003

Dr. Phillip Steindel, Ph.D.
Review Editor of *Journal of Visualized Experiments*
1 Alewife Center, Suite 200
Cambridge, MA 02140

Re: Revisions required for your JoVE submission JoVE61159 - [EMID:656ee77c02225c39]

Dear Dr. Steindel,

Thank you for your response to our manuscript and for providing both editorial and reviewers' comments. We are very grateful to both the editors and the reviewers for the thorough reading of the manuscript and for taking the time to provide thoughtful and insightful comments. We agreed with all the feedback and have modified the paper to the listed specifications. Here, we describe our response to the comments point-by-point.

EDITORIAL COMMENTS

General:

1. Please take this opportunity to thoroughly proofread the manuscript to ensure that there are no spelling or grammar issues.

We have proofread the manuscript to ensure clarity and flow.

2. Please reduce the number of personal pronouns (we, our).

We have removed all usage of personal pronouns in the main text, with the exception of the Acknowledgements section and a few mentions of publications/related work from our lab that were foundational to the development of our current study.

3. Please include all authors' emails in the manuscript itself.

We have added this information to front matter.

4. JoVE cannot publish manuscripts containing commercial language. This includes trademark symbols (™), registered symbols (®), and company names before an instrument or reagent. Please limit the use of commercial language from your manuscript and use generic terms instead. All commercial products should be sufficiently referenced in the Table of Materials and Reagents. For example: Aivia, Eppendorf, Kimwipe

We have modified the main text to avoid commercial language; relevant brand information is in the Table of Materials and Reagents.

Protocol:

1. For each protocol step/substep, please ensure you answer the "how" question, i.e., how is the step performed? Alternatively, add references to published material specifying how to perform the protocol action. If revisions cause a step to have more than 2-3 actions and 4 sentences per step, please split into separate steps or substeps.

We have modified the protocol to include these additional details. Specifically, we have cited Greenspan, 2004 and Hales *et al.,* 2015 to elaborate on standard *Drosophila* husbandry and genetics methods, and we have cited Waters, 2013 to provide further detail on fluorescence microscopy.

Figures:

1. Figure 1C-E does not appear to be cited correctly.

Thank you for pointing this out. We have corrected the text accordingly (lines 332-337).

Discussion:

1. Please revise the Discussion to explicitly cover the following in detail in 3–6 paragraphs with citations: a) Critical steps within the protocol b) Any modifications and troubleshooting of the technique c) Any limitations of the technique

We have expanded our Discussion to emphasize the following issues (examples described).

a) Critical steps – Use of software to ensure unbiased analysis (line 440-441); optimizing quality of the raw data through attention sample preparation and image acquisition (line 455-460); selection of the MT-plus end label and expression method (line 470-471); establishing a uniform genetic background for all experiments (line 471-473).
b) Modifications/troubleshooting - We point out areas where users should modify the protocol as appropriate, such as in reducing detection/tracking of spurious objects (aggregates or noise) (line 444-446) by the software or sample avoiding deterioration due to phototoxicity or chloroform exposure (line 459). We emphasize that these conditions must be empirically determined for each experiment/study. We also point out modifications, such as imaging of additional tissues/cell-types (lines 495-501) or different fluorescent markers (507-509) that can be used to diversify the utilization of this protocol.
c) Limitations – We describe the limitations of the software analysis, e.g. in comparison to plusTipTracker, and the challenges in detecting/tracking comets that move out of focus (line 447-449). We also note caveats associated with chemical anesthetization (lines 464-468) as well as possible artifacts from overexpression of +TIPs or with fluorescent tags in general (lines 474-480).

References:

1. As JoVE does not require an exhaustive set of references, it may be best to reduce the number of papers cited.

We have removed over 30 references to reduce the length of this section.

2. Please do not abbreviate journal titles.

We have corrected the reference format accordingly.

Table of Materials:

1. Please ensure the Table of Materials has information on all materials and equipment used, especially those mentioned in the Protocol.

We have updated the Table to include all materials used in this study.

REVIEWER #1

1. Line 193: Include 221-GAL4 in this procedural step, as both driver lines were utilized in this study.

We have added this information in the protocol (now line 212-213).

2. Line 230: Be more specific with the orientation of the larvae when placing the cover slip. Should the larvae be placed dorsal side up or down? Is there a larval orientation that optimizes both NMJ and dendrite imaging or are there orientations that should be used to optimize NMJ vs. dendrite. Or, if it does not matter, this should be explicitly stated.

We have updated the protocol to explain that the dorsal/ventral orientation does not matter (now line 253-255). We found that both dendrites and NMJ were visible regardless of the larval orientation as long as the correct imaging plane was found. The key difference in difficulty in imaging dendrites and NMJ was due to their relative distance from the cuticle (dendrites are much more superficial and close to the cuticle), as opposed to orientation.

3. Line 291: Provide references for the "published data" to which the comparisons are made.

We have made the appropriate citations (now line 335).

4. Line 308: Authors should state which driver line expresses EB1 at higher levels. This will help readers better interpret the data presented in Figure 3 with respect to how EB1 levels influence

MT dynamics. Citing a previous study that compares 221-GAL4 and elav-GAL4 would be sufficient.

We have modified the Results (lines 352-357) to clarify the intent behind the *elaV Gal4* and *221-Gal4* comparison, i.e. to demonstrate the artifacts that can arise from multiple confounding variables from different genetic backgrounds. To our knowledge, a direct comparison between *elaV-Gal4* and *221-Gal4* driver expression levels has not been performed; however, there are many other differences that may contribute to the differences observed in Figure 3 beyond absolute amounts of EB1 protein. For instance, the drivers have very different distribution patterns: *elaV-Gal4* drives expression pan-neuronally and in neuronal progenitors and glia (Berger *et al*. 2007, Robinow and White, 1991), while *221-Gal4* expression is restricted to sensory dendrites (Grueber *et al*. 2003, Parrish *et al.* 2006). It is also possible that *elaV-Gal4* and *221-Gal4* have different temporal onsets, and additional discrepancies in the genetic background are likely. Given the myriad of ways in which the two drivers might differ, it is difficult to attribute any differences in EB1 to any specific factor, but it is clear that a uniform genetic background is imperative.

5. Fig. 4 - Authors should double-check the significance of Sinuosity and Growth lifetime data in Fig. 4. It is impossible to comment on significance without seeing the raw data, but sinuosity appears to not be significant, especially when compared to the error bars of Growth lifetime, which are presented as not significant.

We have double-checked this statistical calculation and confirm that the significance levels are correct as presented, even if not visually obvious in the figure. For all measurements of significance, we utilized non-parametric tests (Wilcoxon-Mann-Whitney), which, at a conceptual level, tests if the control vs. experimental groups are shifted relative to each other. We included the standard error bars, which is a parametric measurement, primarily to give readers a better sense of our data distribution, as standard error was not actually a part of our significance calculations.

In the case of Sinuosity in Figure 4 in particular, the data for the wild-type was highly right-skewed. Due to this skew, the measures of center of wild-type vs. RNAi appear very similar. However, non-parametric tests, which are more robust when used for non-normal data, revealed that the distributions do in fact differ. We are happy to provide raw data for this measurement upon further request.

6. Line 326: Authors state that "all but one of the parameters (sinuosity) are unique to either…", but Max velocity is also significantly different in both NMJ and dendrite measurement. Authors should rephrase their description of their results to account for this.

Thank you for pointing out this oversight. We have rephrased the text to reflect the results (line 375).

7. Figures 4 and 5: The white arrow is too close to the positive EB1-GFP signal as it partially

overlaps with and occludes the signal in some of the panels. To give readers a better sense of the signal/background that is analyzed, it would be helpful if these white arrows were moved down so that there is no overlap with the signal being analyzed.

We have edited the figures to better depict the EB1-GFP signal.

8. Figures 3-5: Ensure that the line and asterisk delineating significance in the presented graphs are appropriately spaced over the two bars they are comparing.

We have edited the figures to ensure proper alignment.

REVIEWER #2

1. It would be useful to reference the figures shown at the end of the manuscript in the protocol.

We have included references to Figure 1 and 2 in steps 2-5 of the protocol.

2. Protocol 1.4.: The authors may mention that the use of tagged endogenous genes would avoid the mentioned issue of potential gain of function artifacts. In addition, they should also point out that users should be aware that adding tags to proteins may affect or alter the function of the proteins, which can be in part addressed with rescue experiments.

We have elaborated on these considerations and caveats in our Discussion (lines 474-480).

3. Equip set up 2.3: The authors use chloroform anesthetize the larvae. There are studies (e.g.Allison AC, Nunn JF., Lancet. 1968 Dec 21;2(7582):1326-9.) suggesting that chloroform affects MT dynamics and other cytoskeletal elements such as actin. Thus also other methods of immobilization should be considered to confirm exponential results.

We have cited the mentioned paper and elaborated on this issue in our Discussion, and we have proposed alternative methods of immobilization (lines 465-468).

4. Line 228 "step 2" instead of "Step 2"

We have edited this line accordingly.

5. Step 4. Time-lapse confocal imaging of live samples: While no fully clear in the description, its seems that the authors only acquire and analyze live-imaging of one focal plane. As MT comets may project out of the focal plane the authors may mention or discuss that this methods is only of use to 2D analyses or how to deal with 3D analyses.

We have specified that each imaging series (movie) was performed at a single Z-plane in the protocol (step 4) and noted in our Discussion (line 450) that it is not possible to fully track

movement of comets if they move to a different plane. As stated in our title, our protocol describes a 3D imaging strategy since our analysis is performed in two spatial dimensions (X and Y) as well as through time. While we have successfully performed 4D imaging (3D space + timelapse) on synaptic vesicles in the past (Miller *et al.,* 2005), pilot experiments in our current system showed that traversing through Z occurred too slowly to capture the rapid movement of EB1-GFP comets. Thus, while imaging through Z is possible for slower objects such as vesicles, for this study we restricted imaging to a single Z-plane to enable continuous EB1 tracking.

6. Image processing and analysis with Aivia software: It's not clear how a particle section is confirmed with the cursor or if there is an option or how to un-select a particle. "Run the Neuron Particle Tracking software recipe for the selected puncta". There is only one screen shot of the software but from the description it is not clear what "button" to push to run the analyses and how to store the parameters in excel for analysis. It may be useful to either show multiple screen shots or label all the relevant buttons with numbers and have a brief text description of their function in the legend or the protocol.

We have annotated the protocol (step 5) and the Figure 2 image/legend to further explain the user interface. Specifically, left-clicking on the particle allows selection/de-selection. We have annotated the figure to show the “From Beginning” button that should be clicked to run the “Neuron Particle Tracking” recipe. Since we anticipate that readers may have unique needs for their research that are not covered in this protocol, we have also noted in the text that readers may request additional details on software functionality from the authors.